

Electronic Supporting Information

For

Large-scale preparation of heterometallic chalcogenide MnSb_2S_4 monolayer nanosheets with a high visible-light photocatalytic activity for H_2 evolution

Zheguan Lin,^a Shangbo Ning,^a Zhenya Yang,^a Zizhong Zhang,^{*a} Shuping Huang,^{*b} Jinlin Long^a,
Huaxiang Lin^a and Xuxu Wang^{*a}

^aState Key Laboratory of Photocatalysis on Energy and Environment, Research Institute of Photocatalysis,

College of Chemistry, Fuzhou University, P. R. China

E-Mail: z.zhang@fzu.edu.cn; xwang@fzu.edu.cn

^bCollege of Chemistry, Fuzhou University, P. R. China

E-Mail: huangshp@gmail.com

Tel: +86-591-83690891; fax: +86-591-83779251

Experimental

Synthesis of MnSb_2S_4 monolayer

All the reagents used were of analytically pure and commercially available, and used without further purification. MnSb_2S_4 was prepared by calcination of $\text{MnSb}_2\text{S}_4(\text{N}_2\text{H}_4)_2$ (precursor), which was synthesized via low solvothermal method. Firstly, the 0.032g of S, 0.055g of Mn and 0.136g of Sb_2S_3 were adding to a certain amount of hydrazine monohydrate. The mixture was vigorous stirred to acquire homogeneous suspension at room temperature and followed transfer into a Teflon-lined stainless steel autoclave, which was sealed and maintained at 140°C for several days, and then cooled down to room temperature naturally. The resulting solid product was washed with deionized water, absolute acetone and ethanol several times and dried in air at 60°C

for 12h. The XRD patterns (Fig. S1) of as-prepared $\text{MnSb}_2\text{S}_4(\text{N}_2\text{H}_4)_2$ precursors was in accordance with the literature,¹ which reveal that as-prepared $\text{MnSb}_2\text{S}_4(\text{N}_2\text{H}_4)_2$ precursors was successfully synthesized. Finally, the $\text{MnSb}_2\text{S}_4(\text{N}_2\text{H}_4)_2$ was calcined at 500 °C in nitrogen to obtain MnSb_2S_4 monolayers.

Catalyst characterization

The structure of the MnSb_2S_4 was characterized by X-ray diffraction (XRD) on a D/Max2200V/PC X-ray diffractometer with Cu K α radiation ($\lambda=1.54187 \text{ \AA}$). Diffraction patterns were started from 10 ° to 70 ° at a rate of 6 ° min⁻¹. The bilayer morphologies and sizes of the MnSb_2S_4 were inspected by field-emission scanning electron microscopy (FE-SEM, JEOL JSM-6701F and NovaNano SEM 230). The morphology of the MnSb_2S_4 also observed by transmission electron microscopy (Philips-FEI Tecnai F30 300Kw). The photoabsorption of the MnSb_2S_4 was examined by UV-visible diffuse reflectance spectra (PerkinElmer Lambda 950 UV-Vis-NIR). X-ray photoelectron spectroscopy (XPS) measurement was investigated by using the ESCALAB 250 XPS System with a monochromatic source (Al-K α) (15 kV, 150 W, 500 mm, pass energy ¼ 15 eV). All binding energies were referenced to the C1s peak at 284.6 eV of surface adventitious carbon. Thermogravimetric curve (TGA) was performed in the Perkin Elmer thermogravimetric analyzer TGA7 under the nitrogen with the platinum crucible in the temperature range from 25 to 1200 °C with the heating rate of 20 °C min⁻¹. Raman spectrum measurement also was performed in the Renishawn confocal micro Raman spectrometer in Via Reflex with 325nm laser light source. Atomic Force Microscope (AFM) image was obtained via using the Agilent 5500.

Photoelectrochemical test

The Mott–Schottky curve and electrochemical impedance spectroscopy (EIS) were measured under the same conditions by a ZAHNES CAB120 electrochemical System. The test used traditional three-electrode cell in the dark without applied voltage. The Pt electrode was used as a counter electrode. The Ag/AgCl electrode was used as a reference electrode. The MnSb_2S_4 on FTO glass substrate was used as working electrode, which was prepared as following: 10mg of the MnSb_2S_4 powder was dispersed in 1 mL of anhydrous ethanol, then ultrasound and stirring each 1 hour to form homogeneous suspension, which were spread onto the FTO glass substrate and dried in air. The three-electrode was carried out in the 0.2mol/L sodium sulfate electrolyte solution. The frequency of electrochemical work station was performed at 0.5, 1, 1.5 KHz.

Photocatalytic test

The photocatalytic H₂ production reaction was performed in the closed gas circulation system with a side window Pyrex cell reactor. The 50mg of photocatalyst was dispersed in the 100ml aqueous solution containing

CeCl₃·7H₂O(0.03M) as the holes sacrificial reagents. Prior to the photocatalytic reaction, the catalyst system was evacuated three times by a mechanical pump to completely remove air. The suspension was irradiated under the 300 W Xe lamp with the 420 nm cut-off filter and stirred with the magnetic stirrer. During the process, the reaction aqueous solutions were controlled at appropriate temperature by circulating water. The gases in the reaction system were circulated by a microdiaphragm gas pump. The amount of H₂ evolved in the circulation system was analyzed and determined by an online gas chromatography (Shimadzu, GC-8A, TCD, Ar carrier).

The apparent quantum yield for H₂ generation was measured under the similar photocatalytic reaction conduction. The amount of hydrogen production was obtained for 2 h of photocatalytic reaction with band-pass filters of 420, 450, 500, 550, 600 and 650 nm wavelengths, respectively. The light irradiation area was ca. 30.1 cm². The apparent QE was calculated according to follow equation:

$$\begin{aligned} \text{QE} &= \text{number of reacted electrons} / \text{number of incident photons} \times 100\% \\ &= \text{number of evolved H}_2 \text{ molecules} \times 2 / \text{number of incident photons} \times 100\% \end{aligned}$$

Theory calculation of band gap energy of MnSb₂S₄ monolayer

The initial monolayer of MnSb₂S₄ was cut from the fully relaxed bulk MnSb₂S₄ (*mC28*). The lattice parameters are fixed at their bulk values in the monolayer calculations. A vacuum layer of 10 Å is used to remove any spurious interaction between the periodically repeated layers in the layer normal direction. Quantum mechanical calculations were carried out employing both Perdew-Burke-Ernzerhof generalized gradient approximation (PBE-GGA)² and Heyd-Scuseria-Ernzerhof (HSE06)³ screened hybrid exchange–correlation density functionals. The projector augmented wave (PAW) potentials^{4,5} provided in the VASP package^{6,7} were used. All calculations were spin polarized. The energy criterion for self-consistency was set to less than 0.0001 eV/unit cell, and the force criterion in structure relaxation was set to less than 0.001eV/Å. A 4×14×4 Monkhorst-Pack *k* point mesh was used for the calculations on the convention cell of bulk monoclinic MnSb₂S₄ (*Fig. S5a*), and a 4×14×1 one was used for the monolayer (*Fig. S5b-5c*).

The ferromagnetic (FM) and antiferromagnetic (AFM) states of bulk and monolayer MnSb₂S₄ are calculated. The ground spin state of Mn is high spin in both bulk and monolayer. The AFM models are energetically more favorable than the FM models with equal Mn spin directions for both bulk and monolayer. For monolayer MnSb₂S₄, the AFM model with alternating Mn spins along *b* direction is more stable than the AFM model with alternating Mn spins along *a* direction. The calculated magnetic moments of the two Mn are 4.25 and -4.25 μ_B, respectively. The calculated indirect band gaps of monolayer MnSb₂S₄ by GGA-PBE and HSE06 are ~1.0 and ~1.9

eV, respectively, which are larger than the calculated indirect gaps for bulk. The functionals with Hartree–Fock exchange are expected to give more accurate band structures. The HSE06 hybrid functional, which include Hartree–Fock exchange, have the smallest error (0.3 eV) in predicting the gaps of 31 semiconductors.^{8,9} HSE06 was used to obtain the total density of states and partial density of states of MnSb₂S₄ monolayer. The top of valence bands arises from *d* orbitals of Mn and *p* orbitals of S, with a non-negligible contribution from *p* orbitals of Sb. The bottom of conduction bands is mainly due to *p* states of Sb.

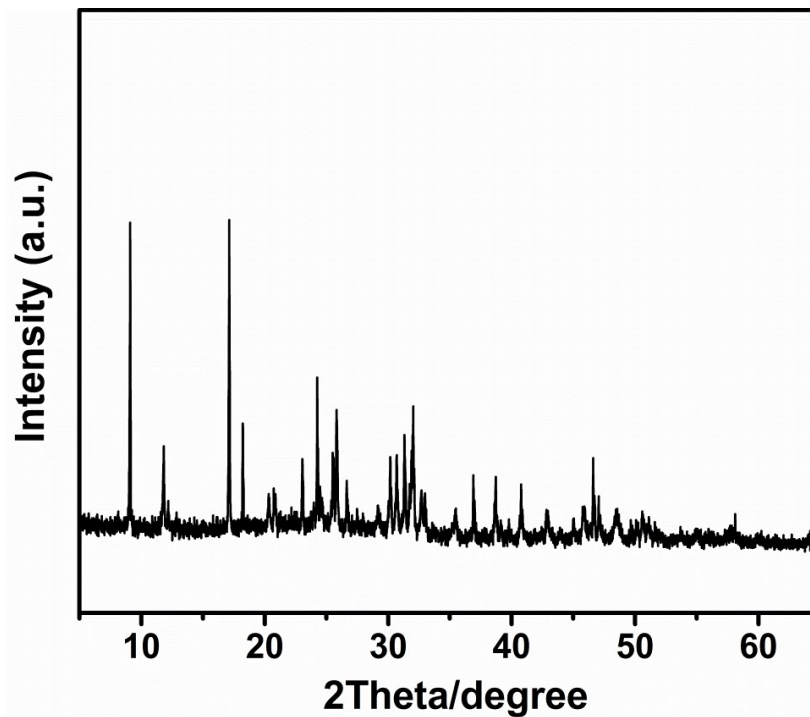


Fig. S1 Power XRD of the as-prepared MnSb₂S₄(N₂H₄)₂ precursors.

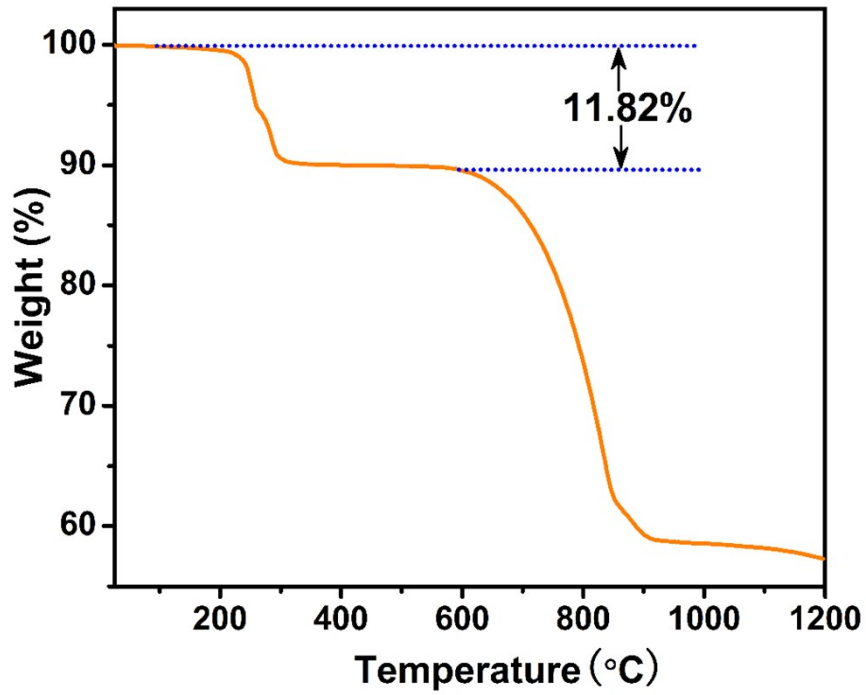


Fig. S2 TG analysis of the as-prepared $\text{MnSb}_2\text{S}_4(\text{N}_2\text{H}_4)_2$ precursors.

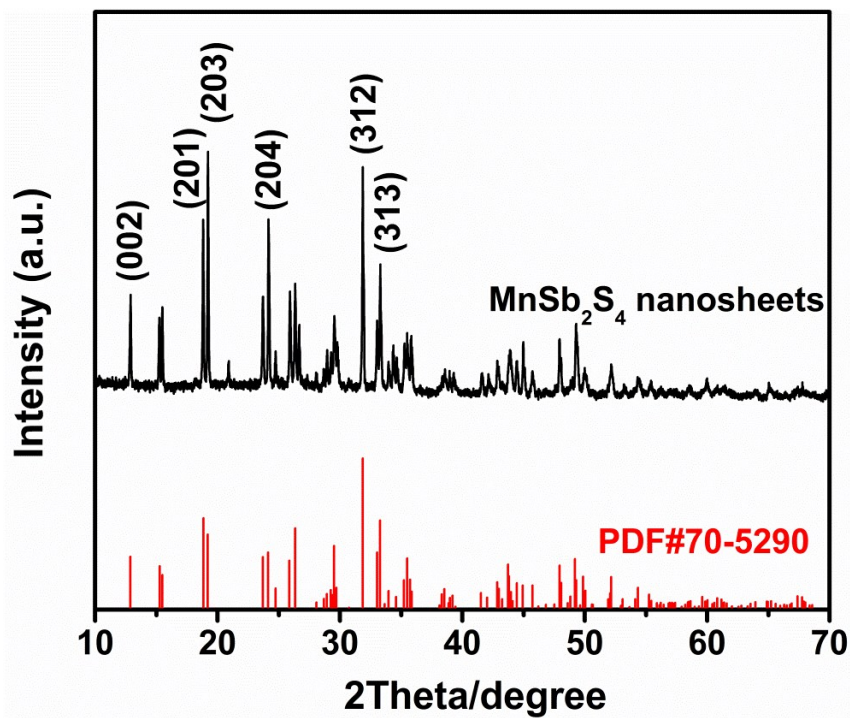


Fig. S3 XRD pattern of MnSb_2S_4 monolayer.

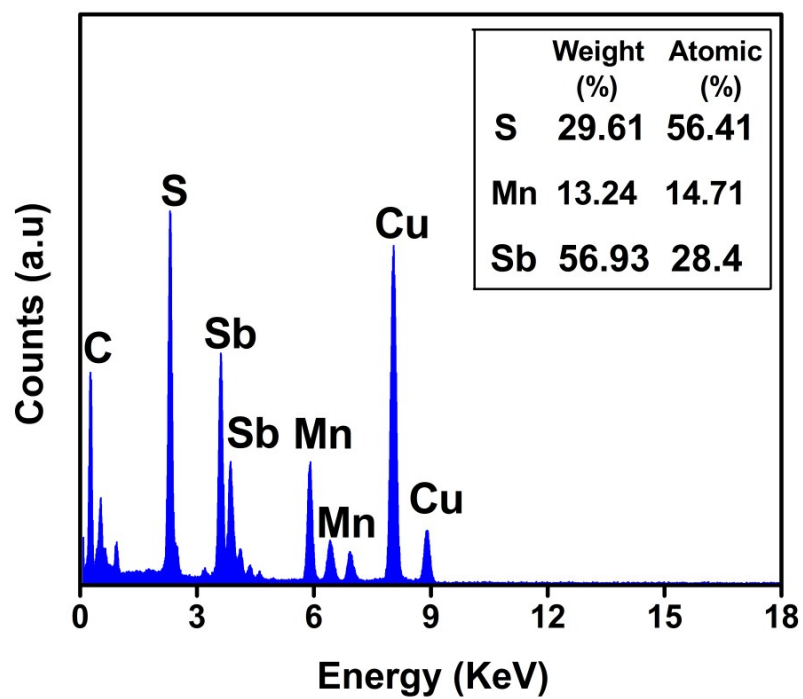


Fig. S4 EDS spectrum of the MnSb_2S_4 monolayer, inset is the corresponding quality and atomic ratio.

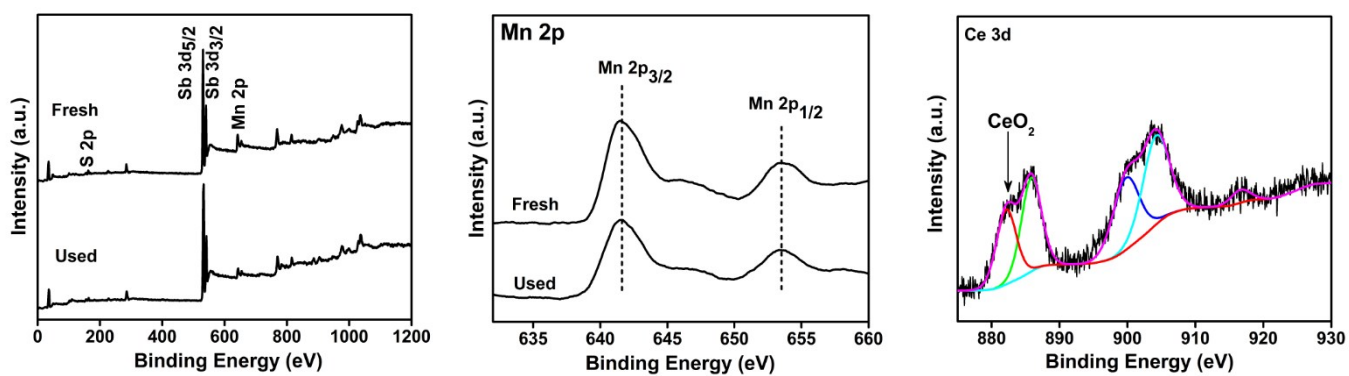


Fig. S5 XPS spectra of MnSb_2S_4 monolayer before (fresh) and after (used) H_2 evolution reaction.

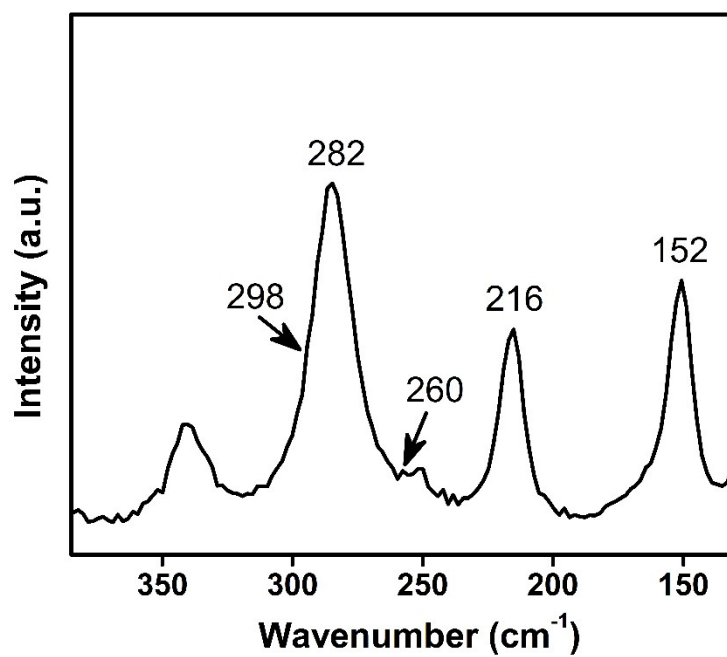


Fig. S6 Raman spectra of the MnSb₂S₄ monolayer.

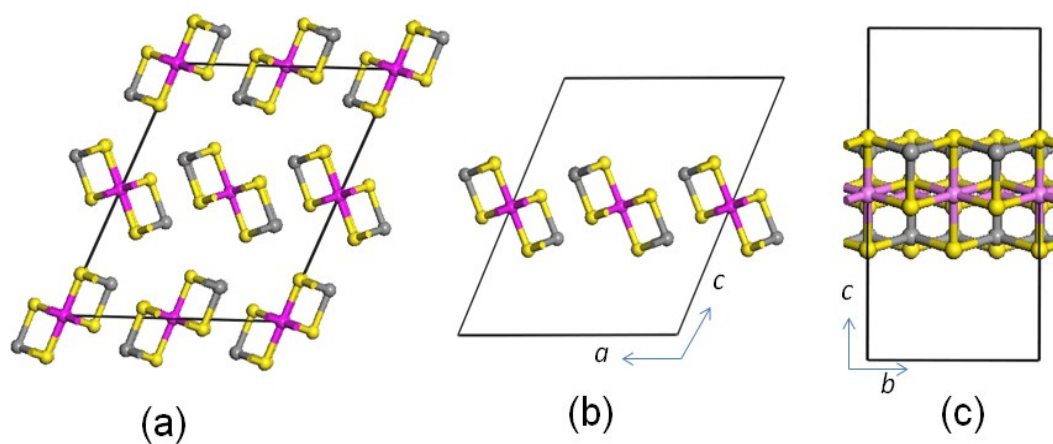


Fig. S7. (a) The convention cell of monoclinic MnSb₂S₄. (b) and (c) Different views of the monolayer MnSb₂S₄. The purple, gray, and yellow balls represent Mn, Sb, and S, respectively.

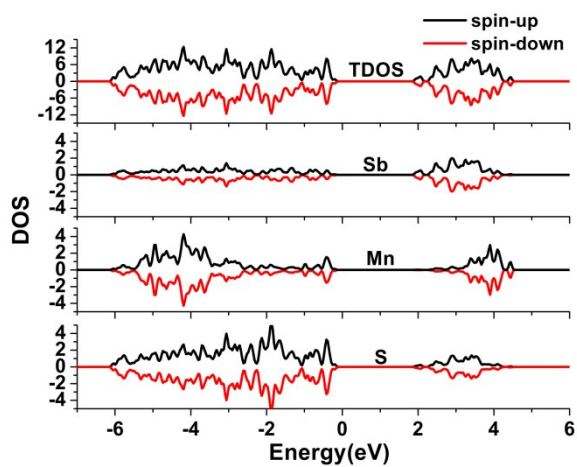


Fig. S8 The total density of states (TDOS) and partial density of states (PDOS) of the monolayer MnSb₂S₄.

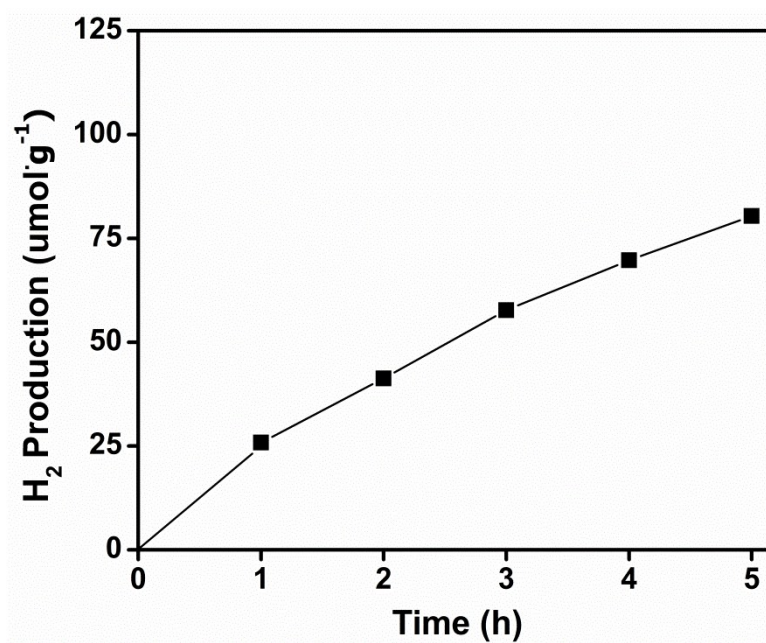


Fig. S9 Photocatalytic H₂ production of MnSb₂S₄ in the presence of methanol as sacrificial reagents.

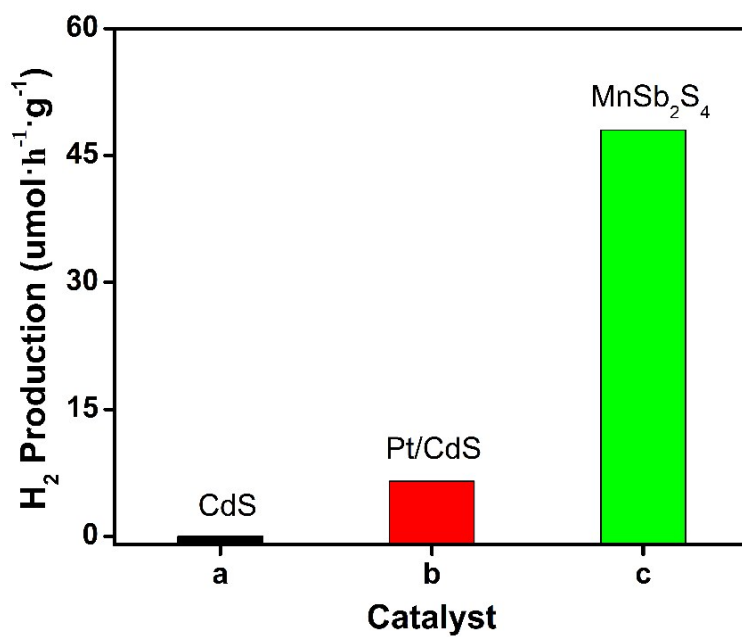


Fig. S10 The comparison of H₂ evolution rates for CdS (a), Pt/CdS (b) and MnSb₂S₄ monolayer (c) photocatalysts.

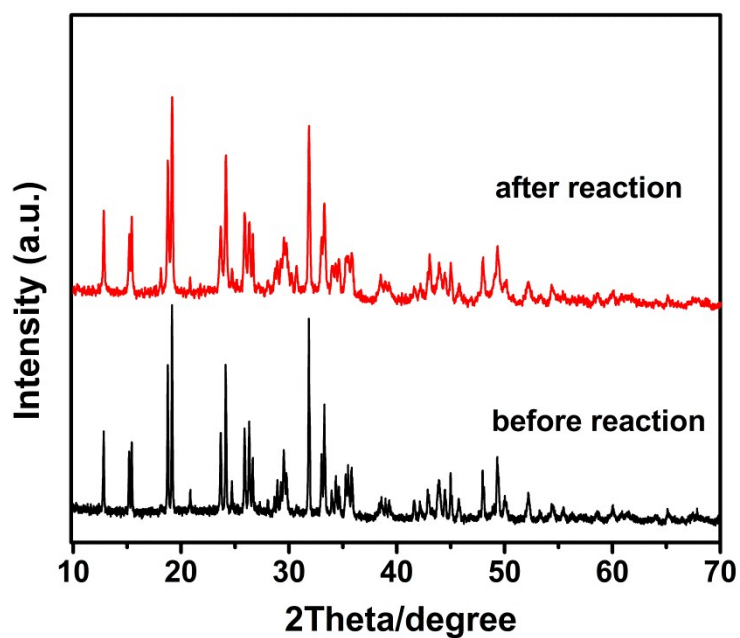


Fig. S11 Power XRD of the as-prepared sample before and after photocatalytic reaction.

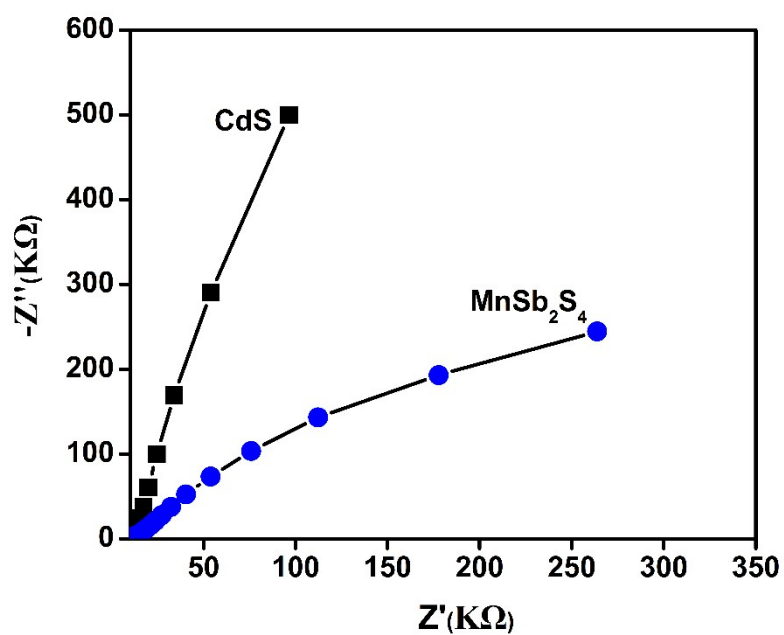


Fig. S12 Comparison of the EIS of MnSb₂S₄ monolayer and CdS photocatalyst in the dark.

Table S1 The states, binding energy and valency of S2p, Mn2p, Sb3d by XPS and the element weight ration of the MnSb₂S₄ monolayer from elemental analysis and ICP.

Element	States	B.E(eV)	Valency	Weight (wt%)
S	2P _{3/2}	161.4	-2	29.3 ^a
	2P _{1/2}	162.5		
Mn	2P _{3/2}	641.7	+2	13.4 ^b
	2P _{1/2}	653.4		
Sb	3d _{5/2}	530.4	+3	57.2 ^b
	3d _{3/2}	539.9		

^a Determined by element analysis

^b Determined by ICP

References

1. Lina Nie.; Wei-Wei Xiong.; Peizhou Li.; Jianyu Han.; Guodong Zhang.; Shengming Yin.; Yanli Zhao.; Rong Xu.; Qichun Zhang. *Journal of Solid State Chemistry*. 2014, 220,118–123.
2. Perdew, J. P.; Burke, K.; Ernzerhof, M. *Phys. Rev. Lett.* 1996, 77,3865.
3. Krukau, A. V.; Vydrov, O. A.; Izmaylov, A. F.; Scuseria, G. E. J. *Chem. Phys.* 2006, 125, 224106.
4. Blochl, P. E. Projector Augmented-Wave Method. *Phys. Rev. B* **1994**, 50, 17953-17978.
5. Kresse, G.; Joubert, D. From Ultrasoft Pseudopotentials to the Projector Augmented-Wave Method. *Phys. Rev. B* **1999**, 59, 1758-1775.
6. Kresse, G.; Furthmuller, J. Efficiency of Ab-Initio Total Energy Calculations for Metals and Semiconductors using a Plane-Wave Basis Set. *Comput. Mat. Sci.* **1996**, 6, 15-50.
7. Kresse, G.; Furthmuller, J. Efficient Iterative Schemes for Ab Initio Total-Energy Calculations using a Plane-Wave Basis Set. *Phys. Rev. B* **1996**, 54, 11169-11186.
8. Peverati, R.; Truhlar, D. G. J. *Chem. Phys.* 2012, 136, 134704
9. Peverati, R.; Truhlar, D. G. *Philos. Trans. R. Soc., A* 2014, 372, 20120476.